Engineering and Technology Journal
Journal homepage: https://etj.uotechnology.edu.iq

Free vibration analysis of aluminum foam metal sandwich panels: a comparative study between numerical and analytical modelling

Zahra K. Hamdan[a,b*], **Sadeq H. Bakhy**[a], **Muhsin J. Jweeg**[c]

[a] Mechanical Engineering Dept., University of Technology-Iraq, Alsina'a street, 10066 Baghdad, Iraq.
[b] Mechanical Engineering Dept., College of Engineering, Mustansiriyah University-Iraq, Baghdad, Iraq.
[c] College of Technical Engineering, Al-Farahidi University, Baghdad, Iraq.
*Corresponding author Email: za.kalid89@gmail.com

HIGHLIGHTS

- The natural frequency of aluminum foam sandwich panels was studied using numerical and analytical methods.
- A CPT-based model was developed for frequency analysis, with Young's modulus computed via Gibson-Ashby.
- FEA in ANSYS validated the analytical results, showing strong agreement between both methods.
- Higher foam density lowers frequencies, while increased Young's modulus enhances stiffness.
- Foam densities of 350–450 kg/m³ optimize stiffness-to-weight balance for aerospace panel design.

Keywords:

Aluminum foam

Sandwich panels

Natural frequency

Finite element analysis (FEA)

Classical plate theory (CPT)

ABSTRACT

This study investigates the natural frequencies and vibrational behavior of aluminum foam sandwich panels by using numerical and analytical methods. The panels consist of an aluminum foam core sandwiched between two aluminum sheets, offering a lightweight yet structurally robust solution, making them ideal for applications in the aerospace and automotive industries. A mathematical model based on classical plate theory (CPT) was developed to compute the natural frequencies of supported rectangular sandwich plates. The Gibson-Ashby equation was employed to estimate the Young's modulus of the aluminum foam core. The analytical model was validated using finite element analysis (FEA) conducted in ANSYS 2021 R1, allowing for a thorough comparison between numerical and analytical results. The results showed strong agreement between the numerical and theoretical analysis, especially at high foam densities. The discrepancies between the numerical simulation and analytical predictions decreased with increasing foam density. For instance, at a density of 850 kg/m³, the difference between the numerical natural frequency (674 Hz) and the analytical prediction (681.75 Hz) was only 1.14%. In contrast, at a lower density of 350 kg/m³, the discrepancy increased to 8.52%, with numerical and analytical frequencies of 739.66 Hz and 808.51 Hz, respectively. This trend can be attributed to the complexities in the material behavior at lower densities, which the analytical model simplifies by neglecting nonlinear deformations and complex stress distributions. As foam density increases, the material exhibits more consistent mechanical properties, resulting in closer alignment between numerical and analytical results. Moreover, higher foam densities contribute to an increase in mass, which negatively affects the natural frequency, causing it to decrease. Conversely, an increase in Young's modulus enhances the stiffness of the material, resulting in higher natural frequencies. Therefore, the optimal foam density range of 350 to 450 kg/m³ is crucial for achieving a good balance between stiffness and weight. Maintaining a lightweight structure while improving stiffness is essential for achieving optimal performance. Consequently, these panels are particularly suitable for applications in the aerospace and automotive sectors that require lightweight, high-performance structures.

1. Introduction

Metallic foams are cellular structures composed of a solid metal matrix interspersed with interconnected voids, resulting in a lightweight and porous material [1-3]. These foam-based sandwich panels offer a high strength-to-weight ratio and demonstrate greater

http://doi.org/10.30684/etj.2024.153779.1821
Received 21 September 2024; Received in revised form 23 October 2024; Accepted 20 November 2024; Available online 05 January 2025
2412-0758/University of Technology-Iraq, Baghdad, Iraq

energy storage capacity compared to conventional panels [4,5]. These foams are utilized in various engineering applications, particularly in industries such as aerospace, automotive, and construction [6,7].

Sandwich structures with multiple layers and diverse core materials have improved mechanical and dynamic properties in recent years. Initially, fiber materials were reinforced to increase durability and strength, and nanomaterials were added to improve microscopic physical properties. This improved composite structure's static and dynamic performance in various applications [8-10]. Recently, research has focused on improving composite plate structural properties by increasing static and dynamic properties, reducing weight, and increasing the strength-to-weight ratio. Reinforcing polymer core materials and using functionally graded materials in solid and porous structures have achieved this [11,12].

Materials that are lightweight and mechanically efficient are suitable for automotive applications. Core density affects mechanical behavior, with higher densities increasing bending strength but decreasing energy absorption [13]. AFS panels are ideal for automotive battery boxes due to their sound absorption and fire resistance [14]. Recent studies show that steel-aluminum foam-steel sandwich panels are strong and stiff enough for lightweight structural systems [15].

Innovative methods to improve the performance of these advanced composite materials require ongoing research [16]. Aluminum foam core sandwich panels (AFSP) with reinforced blankets are used in aerospace applications to provide structural robustness and protection against micrometeoroids and orbital debris [17]. Superior mechanical properties and a lightweight design make these panels suitable for structural applications that require lightness and strength.

Recent studies have used numerical and analytical modeling to analyze the free vibration sandwich panel. These studies examined how material properties, geometric configurations, and boundary conditions affect vibration. In this context, several techniques have been used to study the behavior of sandwich panels. For example, the focus has been on functionally graded materials (FGMs) and their effects on vibration behavior; Mouthanna et al. [18], developed an analytical model for cylindrical panels made of porous FGMs using the Galerkin technique and finite element analysis (FEA) to evaluate the effect of porosity and material thickness on the free vibration characteristics. In addition, Amir et al. [19], studied functionally graded porous panels considering geometric nonlinearity. Emad et al. [20], used a new analytical model to conduct the free vibration analysis of a supported rectangular functionally graded sandwich plate. The core metal properties are assumed to be porosity-dependent and graded in the thickness direction according to a simple power-law distribution of constituent volume fractions using higher-order nonlinear envelope theory and stochastic analysis to understand the effects of boundary conditions and porosity on the vibration behavior. A numerical model employing the homogenization method for sandwich composite panels has also been proposed, facilitating efficient vibration analysis through finite element analysis, and has been validated against conventional 3D models [21]. In addition to conventional sandwich panels, the free vibration analysis of sandwich structures with metal foam cores has been extensively studied using both numerical and analytical methods. These studies aimed to enhance the structural performance, comprehend the dynamic behavior of these structures, and verify the models by comparing them with experimental data. Jamaluddin [22], used finite element analysis (FEA) to improve the natural frequencies of sandwich foam core structures, and the results were validated through experimental comparisons. Wang et al. [23], also studied different pore distributions, including gradient distributions, that were created in novel porous materials. Mechanical tests assessed fundamental material properties, including Young's modulus. For the purpose of assessing the impact of various parameters on the vibration characteristics of curved sandwich panels with composite nano face sheets, Badarloo and Salehipour devised closed-loop analytical solutions [24]. Another study by Rahmani et al. [25], explored the nucleation of syntactic foams using higher-order sandwich panel theory, providing insights into the eigenmodes of supported beams.

Although previous studies have addressed the experimentality of metallic foam-based sandwich panels, this research focuses on the free vibration analysis of aluminum foam sandwich panels using both numerical and analytical methods. The distinguishing feature of the current study is the integration of classical plate theory (CPT) with finite element analysis (FEA), combined with the development of a mathematical model based on CPT for foam-based sandwich structures to predict natural frequencies. This represents a novel contribution not previously explored in depth in the existing literature. Additionally, the current study comprehensively compares the numerical and analytical results across various foam densities. Many previous studies have not focused on such a precise comparison between these two approaches.

2. Materials and method

Consider a thin rectangular sandwich panel with an aluminum metal foam core consisting of two aluminum metal sheets. The length, breadth, and thickness of the sandwich are represented by the symbols a, b, and h, respectively. To characterize the movement of the panel, a Cartesian coordinate system (x, y, and z) is used on the central surface of the sandwich, with x and y representing the in-plane coordinates and z representing the out-of-plane coordinates of the plate, as shown in Figure 1. Two 1mm-thick aluminum metal plates surround the metal foam. Through the utilization of the classical plate theory (CPT), it is possible to obtain the equation of motion so the natural frequency of the sandwich can be calculated. In this work, aluminum foams of different densities with a constant thickness of 10 mm were used, and the aluminum foam was treated as homogeneous in properties so that it could be considered homogeneous. In some models and studies, aluminum foam is treated as an approximately homogeneous material. This means that the material is considered to have uniform mechanical properties (such as density, modulus of elasticity, and tensile strength) throughout the sample rather than taking into account the cellular structure or gaps. This approximation is used to simplify calculations in analytical or numerical models when the fine details of the internal structure of the foam are unnecessary or too complex to include in the analysis [26, 27]. Metal foams can be considered as homogeneous materials to simplify numerical modeling, especially in applications where general mechanical properties such as stiffness and density are more important than microscopic details [28].

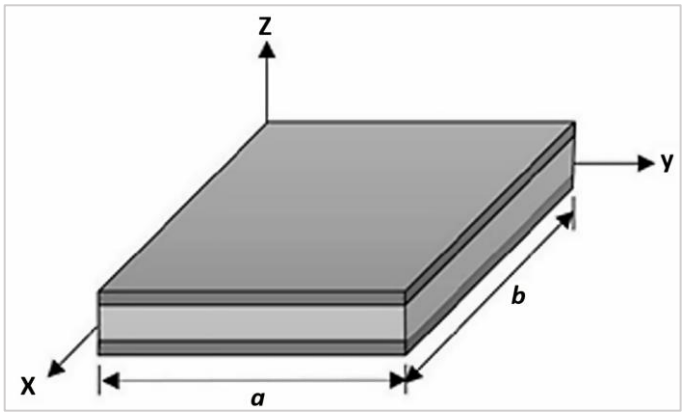

Figure 1: Cartesian coordinate system

The mechanical properties (i.e., Young's modulus) of the aluminum foam were theoretically determined based on the foam's density and the properties of the solid material, using the appropriate theoretical model, the Gibson-Ashby Equation. This equation is used to calculate Young's modulus of closed-cell foams based on the relative density of the foam. The basic formula is explained in Equation 1 [26]:

$$E_f = E_s \left(\frac{\rho_f}{\rho_s}\right)^n \quad (1)$$

where: E_f , E_s is the Young's modulus of the foam and the solid material, ρ_f , ρ_s is the density of the foam and the solid material, and n is constant and equal to 2 for closed-cell.

3. Analytical solution

The governing differential equations that describe the vibration behavior of sandwich structures were derived. The approach aligns with Kirchhoff's theory, commonly referred to as the Classical Plate Theory, which applies to thin plates. The following are the assumptions of the linear elastic small deflection theory for thin plates [29]. The plate thickness (h) is small compared to its lateral dimensions:

1) The plate material is assumed to be elastic, homogeneous, and isotropic.
2) Initially, the plate is flat.
3) The deflection of the mid-plane is small, leading to a minimal slope of the deflected surface, making the square of the slope negligible compared to unity.
4) Lines that are initially perpendicular to the mid-plane remain straight and perpendicular during deformation, and their length does not change. Vertical shear strains (γ_{xz} & γ_{yz}) are considered negligible, as is the normal stress component (ε_{zz}).
5) The normal stress through the thickness (σ_{zz}) is small compared to other stress components and can be neglected in stress-strain relationships.
6) Since the displacements of the plate are moderate, it is assumed that the central surface remains unstressed after bending.

These assumptions simplify the mathematical modeling and allow for a more straightforward analysis of the plate's vibration behavior under small deflections as mentioned in Equation 2 to Equation 4:

$$D\nabla^2\nabla^2 w(x,y,t) = p(x,y,t) - \rho h \frac{\partial^2 w}{\partial t^2}(x,y,t) \quad (2)$$

$$\frac{\partial^2 M_{xx}}{\partial x^2} + 2\frac{\partial^2 M_{xy}}{\partial x\,\partial y} + \frac{\partial^2 m_{yy}}{\partial y^2} + \rho h \frac{\partial^2 \omega}{\partial t^2} = p_z \quad (3)$$

$$\frac{\partial^2 M_{xx}}{\partial x^2} + 2\frac{\partial^2 M_{xy}}{\partial x\,\partial y} + \frac{\partial^2 M_{yy}}{\partial y^2} + \rho h \frac{\partial^2 \omega}{\partial t^2} = 0 \quad \text{(free vibration)} \quad (4)$$

where M_x, M_y, and M_{xy} are the bending and twisting moments per unit length of the plate [23], as shown in Figure 2. According to Kirchhoff's hypothesis, the strain displacement for plates can be expressed in terms of the transverse displacement of the mid-surface of the plate as explained in Equation 5. This displacement occurs due to the stress experienced by the elastic body under an applied load.

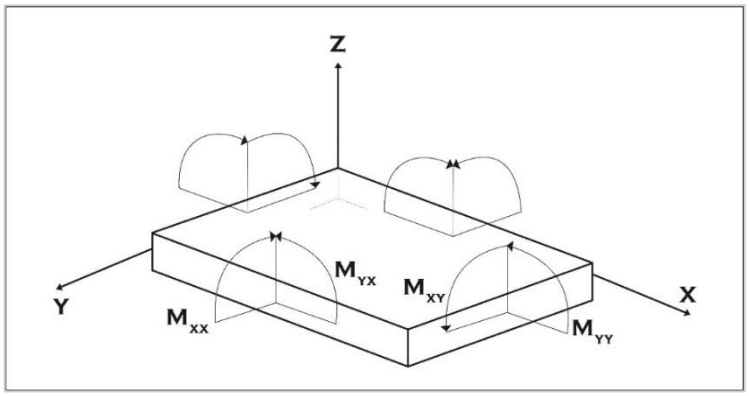

Figure 2: Moments on flat sandwich layer

$$\begin{Bmatrix}\varepsilon_{xx}\\ \varepsilon_{yy}\\ \varepsilon_{xy}\end{Bmatrix}=\begin{Bmatrix}\frac{\partial u}{\partial x}\\ \frac{\partial u}{\partial y}\\ \frac{\partial u}{\partial y}+\frac{\partial u}{\partial x}\end{Bmatrix}=\begin{Bmatrix}\frac{\partial w_0}{\partial x}-z\frac{\partial^2 w}{\partial x^2}\\ \frac{\partial w_0}{\partial y}-z\frac{\partial^2 w}{\partial y^2}\\ \frac{\partial w_0}{\partial y}+\frac{\partial w_0}{\partial x}-2z\frac{\partial^2 w}{\partial x\,\partial y}\end{Bmatrix} \quad (5)$$

Stresses can be described as transverse displacements through the stress-strain relationships [29]. The normal and shear stresses acting on the plate are represented by σ_x , σ_y and σ_{xy}, respectively as explained in Equation 6. The mechanical properties of plate materials sections in the x and y directions are $E_{xx}, E_{yy}, G_{xy}, v_{xy}, v_{yx}$ and $w_{(x,y,t)}$ is the deflection of the plate in the z-direction.

$$\sigma_x=-z\left(\frac{E_{xx}}{1-v_{xy}v_{yx}}\frac{\partial w_{(x,y,t)}}{\partial x^2}^2+\frac{E_{yy}\vartheta_{xy}}{1-v_{xy}v_{yx}}\frac{\partial w_{(x,y,t)}}{\partial y^2}^2\right)$$

$$\sigma_y=-z\left(\frac{E_{xx}\vartheta_{yx}}{1-v_{xy}v_{yx}}\frac{\partial w_{(x,y,t)}}{\partial x^2}^2+\frac{E_{yy}}{1-v_{xy}v_{yx}}\frac{\partial w_{(x,y,t)}}{\partial y^2}^2\right)$$

$$\sigma_{xy}=-2ZG_{xy}\frac{\partial w_{(x,y,t)}}{\partial x\partial y}^2 \quad (6)$$

Equation (7) provides moments obtained by integrating over layer thickness. Bending and twisting moments are computed by correlating stress values with the thickness of the plate (or each layer). These moments will be used in subsequent equations for motion and equilibrium. Equation (8) integrates layer density, which is likewise covered by this process. For equations involving motion and vibration, this value is essential. The behavior of the plate or sandwich panel is theoretically described by the combination of Equations (7, 8) and the stress equations. In the sections that follow, layer stresses will be computed using these relationships.

$$\begin{Bmatrix}M_x\\ M_y\\ M_{xy}\end{Bmatrix}=\int_{-z/2}^{z/2}\begin{Bmatrix}\sigma_x\\ \sigma_y\\ \tau_{xy}\end{Bmatrix}z \quad (7)$$

$$\rho h=\int_{-h/2}^{h/2}\rho\ \partial z \quad (8)$$

Homogeneous materials, the mechanical properties are represented as follows:

$E_{xx}=E_{yy}=E$ & $G_{xy}=G=\frac{E}{2(1+v)}$ Also $v_{xy}=v$, thus, stress relationships in Equation 6 become:

$$\begin{Bmatrix}\sigma_{xx}\\ \sigma_{yy}\\ \sigma_{xy}\end{Bmatrix}=-z\begin{Bmatrix}\frac{E}{1-v^2}\left(\frac{\partial^2 w}{\partial x^2}+v\frac{\partial^2 w}{\partial y^2}\right)\\ \frac{E}{1-v^2}\left(v\frac{\partial^2 w}{\partial x^2}+\frac{\partial^2 w}{\partial y^2}\right)\\ \frac{E}{(1+v)}\frac{\partial^2 w}{\partial x\,\partial y}\end{Bmatrix} \quad (9)$$

A sandwich plate consists of three layers: an upper face with a thickness h_{up}, a lower face with a thickness h_{lp}, and a thick core (metal foam) in between with a thickness h_f. This configuration is typically used to provide structural strength and stiffness while minimizing weight, as shown in Figure 3.

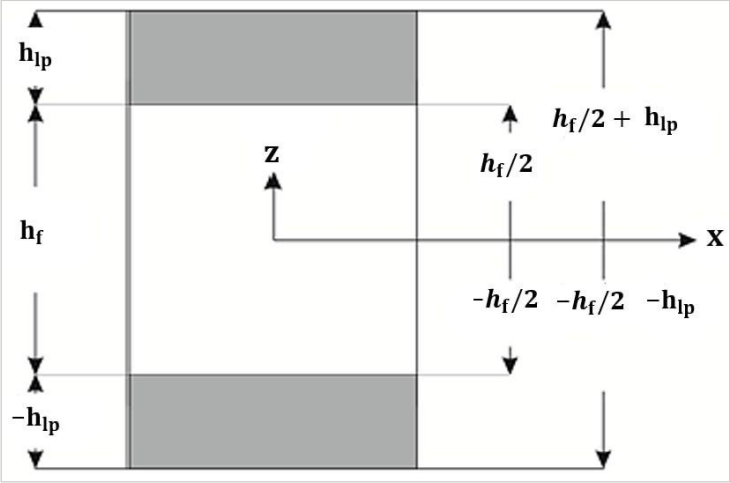

Figure 3: The layers of the sandwich plate layers

The stress relationships for each layer of the sandwich panel can be expressed in the sandwich panel can be expressed in terms of the properties of each layer in Equation 10 to Equation 16. The properties of the upper face: the upper face is made of homogenous aluminum in this study.

$E_{xy} = E_{yx} = E_{up} = E_{upAL}$, $v_{xy} = v_{yx} = v_{upAL}$, $\rho = \rho_{upAL}$, h_{up} = thick of upper face

$$G_{xy} = G_{upAL} = \frac{E_{upAL}}{2(1 + v_{upAL})}$$

$$\begin{Bmatrix} \sigma_{xx} \\ \sigma_{yy} \\ \sigma_{xy} \end{Bmatrix} = -z \begin{Bmatrix} \frac{E_{upAL}}{1-v_{upAL}} \left(\frac{\partial^2 w}{\partial x^2} + v_{upAL} \frac{\partial^2 w}{\partial y^2} \right) \\ \frac{E_{upAL}}{1-v_{upAL}^{\,2}} \left(v_{upAL} \frac{\partial^2 w}{\partial x^2} + \frac{\partial^2 w}{\partial y^2} \right) \\ \frac{E_{upAL}}{(1+v_{upAL})} \frac{\partial^2 w}{\partial x \, \partial y} \end{Bmatrix} \quad (10)$$

$$\begin{Bmatrix} M_x \\ M_y \\ M_{xy} \end{Bmatrix} = \int_{\frac{h_f}{2}}^{\frac{h_f}{2}+h_{up}} \begin{Bmatrix} \sigma_x \\ \sigma_y \\ \tau_{xy} \end{Bmatrix} z \quad (11)$$

The properties of the lower face (same upper): the lower face is made of homogenous aluminum in this study

$E_{xy} = E_{yx} = E_{lpAL}$, $v_{xy} = v_{yx} = v_{lpAL}$, $\rho = \rho_{lpAL}$, h_{lp}= thick of lower face

$$G_{xy} = G_{up} = \frac{E_{lpAL}}{2(1 + v_{lpAL})}$$

$$\begin{Bmatrix} \sigma_{xx} \\ \sigma_{yy} \\ \sigma_{xy} \end{Bmatrix} = -z \begin{Bmatrix} \frac{E_{lpAL}}{1-v_{lpAL}} \left(\frac{\partial^2 w}{\partial x^2} + v_{lpAL} \frac{\partial^2 w}{\partial y^2} \right) \\ \frac{E_{upAL}}{1-v_{lpAL}^{\,2}} \left(v_{lpAL} \frac{\partial^2 w}{\partial x^2} + \frac{\partial^2 w}{\partial y^2} \right) \\ \frac{E_{lpAL}}{(1+v_{lpAL})} \frac{\partial^2 w}{\partial x \, \partial y} \end{Bmatrix} \quad (12)$$

$$\begin{Bmatrix} M_x \\ M_y \\ M_{xy} \end{Bmatrix} = \int_{-\frac{h_f}{2}-h_{lp}}^{-\frac{h_f}{2}} \begin{Bmatrix} \sigma_x \\ \sigma_y \\ \tau_{xy} \end{Bmatrix} z \quad (13)$$

It is important to observe that both the upper and lower faces are constructed from the same material, thus:

$$E_{lpAL}=E_{upAL}=E_{AL}, v_{lpAL}=v_{upAL}=v_{AL}\ , \rho_{lpAL}=\rho_{upAL}=\rho_{AL}\ , h_{lp}=h_{up}=h_{AL}$$

$$G_{upAL}=G_{lpAL}=G_{AL}=\frac{E_{AL}}{2(1+v_{AL})}$$

$$\begin{Bmatrix}\sigma_{xx}\\ \sigma_{yy}\\ \sigma_{xy}\end{Bmatrix}=-z\begin{Bmatrix}\frac{E_{AL}}{1-v_{AL}}\left(\frac{\partial^2 w}{\partial x^2}+v_{AL}\frac{\partial^2 w}{\partial y^2}\right)\\ \frac{E_{AL}}{1-{v_{AL}}^2}\left(v_{AL}\frac{\partial^2 w}{\partial x^2}+\frac{\partial^2 w}{\partial y^2}\right)\\ \frac{E_{AL}}{(1+v_{AL})}\frac{\partial^2 w}{\partial x\,\partial y}\end{Bmatrix} \quad (14)$$

The properties of metal foam core : the metal foam core is made from aluminum, which is considered a homogenous material.

$$E_{xy}=E_{yx}=E_f,\ \ v_{xy}=v_{yx}=v_f\ , \rho=\rho_f\ , h_f=\text{thickness of foam}\quad G_{xy}=G_f=\frac{E_f}{2(1+v_f)}$$

$$\begin{Bmatrix}\sigma_{xx}\\ \sigma_{yy}\\ \sigma_{xy}\end{Bmatrix}=-z\begin{Bmatrix}\frac{E_f}{1-v_f}\left(\frac{\partial^2 w}{\partial x^2}+v_f\frac{\partial^2 w}{\partial y^2}\right)\\ \frac{E_f}{1-{v_f}^2}\left(v_f\frac{\partial^2 w}{\partial x^2}+\frac{\partial^2 w}{\partial y^2}\right)\\ \frac{E_f}{(1+v_f)}\frac{\partial^2 w}{\partial x\,\partial y}\end{Bmatrix} \quad (15)$$

$$\begin{Bmatrix}M_x\\ M_y\\ M_{xy}\end{Bmatrix}=\int_{-\frac{h_f}{2}}^{\frac{h_f}{2}}\begin{Bmatrix}\sigma_x\\ \sigma_y\\ \tau_{xy}\end{Bmatrix}z \quad (16)$$

Then, the total moment acting on the metal foam sandwich panel is calculated by summing the bending moments for each layer as explained in Equation 17. Also, the total density value of the sandwich panel represents the sum of the densities of all layers as explained in Equation 18:

$$\begin{aligned}M_x^{total}&=M_x upper\ layer\ +M_x foam\ +M_x lower\ \text{layer}\\ M_y^{total}&=M_y upper\ layer\ +M_y foam\ +M_y\ lower\ \text{layer}\\ M_{xy}^{total}&=M_{xy} upper\ layer\ +M_{xy} foam\ +M_{xy} lower\ \text{layer}\end{aligned} \quad (17)$$

$$\rho\ =(\rho h\ upper\ layer\ +\ \rho h\ foam\ +\ \rho h\ lower\ \text{layer})/h^{total} \quad (18)$$

Substitute Equations 11, 13, and 16 in to Equation 17 to determine the total moments in the sandwich panel, as represented by Equations 19, 20, and 21.

$$M_x^{total}=\frac{-E_{lpAL}}{1-{v_{lpAL}}^2}\left(\frac{\partial {w_{(x,y,t)}}^2}{\partial x^2}+v_{lpAL}\frac{\partial {w_{(x,y,t)}}^2}{\partial y^2}\right)\int_{-h_f/2-h_{lpAL}}^{-h_f/2} z^2\,dz+\frac{-E_f}{1-{v_f}^2}\left(\frac{\partial {w_{(x,y,t)}}^2}{\partial x^2}+v_f\frac{\partial {w_{(x,y,t)}}^2}{\partial y^2}\right)\int_{-h_f/2}^{h_f/2} z^2\,dz+\frac{-E_{upAL}}{1-{v_{upAL}}^2}\left(\frac{\partial {w_{(x,y,t)}}^2}{\partial x^2}+v_{upAL}\frac{\partial {w_{(x,y,t)}}^2}{\partial y^2}\right)\int_{\frac{h_F}{2}}^{\frac{h_F}{2}+h_{up}} z^2\,dz \quad (19)$$

$$M_y^{total}=\frac{-E_{lpAL}}{1-{v_{lpAL}}^2}\left(v_{lpAL}\frac{\partial {w_{(x,y,t)}}^2}{\partial x^2}+\frac{\partial {w_{(x,y,t)}}^2}{\partial y^2}\right)\int_{-h_f/2-h_{lpAL}}^{-h_f/2} z^2\,dz+\frac{-E_f}{1-{v_f}^2}\left(v_f\frac{\partial {w_{(x,y,t)}}^2}{\partial x^2}+\frac{\partial {w_{(x,y,t)}}^2}{\partial y^2}\right)\int_{-h_f/2}^{h_f/2} z^2\,dz+\frac{-E_{upAL}}{1-{v_{upAL}}^2}\left(v_{upAL}\frac{\partial {w_{(x,y,t)}}^2}{\partial x^2}+\frac{\partial {w_{(x,y,t)}}^2}{\partial y^2}\right)\int_{\frac{h_f}{2}}^{\frac{h_f}{2}+h_{upAL}} z^2\,dz \quad (20)$$

$$M_{xy}^{total}{}_{xy}=\frac{-E_{lpAL}}{1+v_{lpAL}}\frac{\partial {w_{(x,y,t)}}^2}{\partial x\partial y}\int_{-h_f/2-h_{lpAL}}^{-h_f/2} Z^2\,dz+\frac{-E_f}{1+v_f}\frac{\partial {w_{(x,y,t)}}^2}{\partial x\partial y}\int_{-h_f/2}^{-h_f/2} Z^2\,dz+\frac{-E_{upAL}}{1+v_{upAL}}\frac{\partial {w_{(x,y,t)}}^2}{\partial x\partial y}\int_{\frac{h_f}{2}}^{\frac{h_f}{2}+h_{upAL}} Z^2\,dz \quad (21)$$

To simplify the calculation process, let

$$A_f = \frac{E_f h_f^3}{12(1-v_f{}^2)} \tag{22}$$

$$A_{up} = \frac{E_{upAL}}{3(1-v_{upAL}{}^2)}\left(h_{upAL}^3 + \frac{3h_{upAL}^2 h_f}{2} + \frac{3h_f^2 h_{upAL}}{4}\right) \tag{23}$$

$$A_{lp} = \frac{E_{lpAL}}{3(1-v_{lpAL}{}^2)}\left(h_{lpAL}^3 + \frac{3h_{lpAL}^2 h_f}{2} + \frac{3h_f^2 h_{lpAL}}{4}\right) \tag{24}$$

$E_{upAL}=E_{lpAL}=E_{AL}$, $v_{upAL}=v_{lpAL}=v_{AL}$, $h_{upAL}=h_{lpAL}=h_{AL}$ and $A_{up}=A_{lp}=A_{AL}$

Substitute Equations 22, 23, and 24 into Equations 19, 20, and 21. As a result, the total moment is simplified to:

$$M_x^{total} = -(2A_{AL} + A_f)\frac{\partial w_{(x,y,t)}{}^2}{\partial x^2} - (2A_{AL}v_{AL} + \boldsymbol{A_f}v_f)\frac{\partial w_{(x,y,t)}{}^2}{\partial y^2} \tag{25}$$

$$M_y^{total} = -(2A_{AL}v_{AL} + \boldsymbol{A_f}v_f)\frac{\partial w_{(x,y,t)}{}^2}{\partial x^2} - (2A_{AL} + A_f)\frac{\partial w_{(x,y,t)}{}^2}{\partial y^2} \tag{26}$$

$$M_{xy}^{total} = -(2A_{AL}(1-v_{AL}) + A_f(1-v_f))\frac{\partial w_{(x,y,t)}{}^2}{\partial x \partial y} \tag{27}$$

Substitute Equations 25, 26, and 27 in the equation of motion Equation 4:

$$-(2A_{AL} + A_f)\frac{\partial^4 w_{(x,y,t)}}{\partial x^4} - (2A_{AL}v_{AL} + A_f v_f)\frac{\partial^4 w_{(x,y,t)}}{\partial x^2 \partial y^2} - 2(2A_{AL}(1-v_{AL}) + A_f(1-v_f))\frac{\partial^4 w_{(x,y,t)}}{\partial x^2 \partial y^2} - (2A_{AL}v_{AL} + A_f v_f)\frac{\partial^4 w_{(x,y,t)}}{\partial x^2 \partial y^2} - (2A_{AL} + A_f)\frac{\partial^4 w_{(x,y,t)}}{\partial y^4} - (2\rho_{AL}h_{AL} + \rho h_f)\frac{\partial w_{(x,y,t)}{}^2}{\partial t^2} = 0 \tag{28}$$

Equation 28 can be solved using the method of separation of variables by assuming a deflection function as specified in Equation 29 [30]:

$$w(x,y,t) = w(x,y)\cdot w(t) \tag{29}$$

Consider a rectangular plate with a length (a) and width (b), where all four edges are supported, as shown in Figure 2. To evaluate the plate's deflection behavior as a function of the x and y directions, satisfying the boundary conditions w=0 and M=0 on all four edges, the deflection equation of the plate as a function of x and y is given by Equation 30 [31], as shown in Figure 4.

$$\left(\frac{\partial^2 W_2}{\partial x^2} + v\frac{\partial^2 W_2}{\partial y^2}\right)\Big|_{(a,y)} = 0 \text{ and } W(a,y) = 0\,, \left(\frac{\partial^2 W_2}{\partial x^2} + v\frac{\partial^2 W_2}{\partial y^2}\right)\Big|_{(0,y)} = 0 \text{ and } W(0,y) = 0$$
$$\left(\frac{\partial^2 W_2}{\partial y^2} + v\frac{\partial^2 W_2}{\partial x^2}\right)\Big|_{(x,b)} = 0\,, W(x,b) = 0\,, \left(\frac{\partial^2 W_2}{\partial y^2} + v\frac{\partial^2 W_2}{\partial x^2}\right)\Big|_{(x,0)} = 0 \textit{ and } W(x,0) = 0 \tag{30}$$

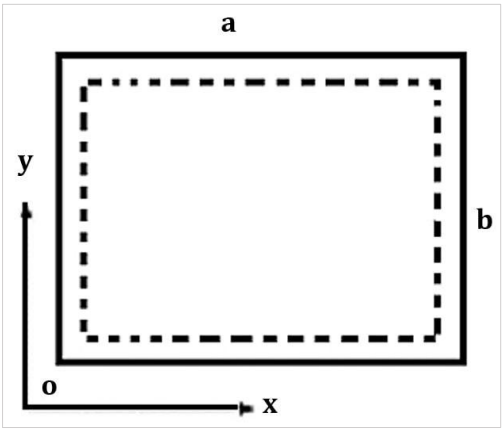

Figure 4: Rectangular plate ($a \times b$) simply supported in all directions

When Applying the four boundary conditions, the displacement equation can be written as follows:

$$\mathrm{w(x,y)} = \sin\frac{\mathrm{m}\pi x}{a}\cdot\sin\frac{\mathrm{n}\pi y}{\mathrm{b}}(\mathrm{m,n} = 1,2,3\ldots\ldots\ldots) \tag{31}$$

By deriving Equation 31 with respect to the second derivative in the x-direction, y-direction, and XY, the fourth-order Equation 28 can be solved:

$$\frac{\partial w_{(x,y,t)}}{\partial x^4} = \left(\frac{m\pi}{a}\right)^4 \sin\frac{m\pi x}{a}\sin\frac{n\pi y}{b}\quad w_{(t)}$$

$$\frac{\partial w_{(x,y,t)}}{\partial y^4} = \left(\frac{n\pi}{b}\right)^4 \sin\frac{m\pi x}{a}\sin\frac{n\pi y}{b}\quad w_{(t)}$$

$$\frac{\partial w_{(x,y,t)}}{\partial x^4 \partial y^2} = \left(\frac{m\pi}{a}\right)^2\left(\frac{n\pi}{b}\right)^2 \sin\frac{m\pi x}{a}\sin\frac{n\pi y}{b}\quad w_{(t)} \tag{32}$$

$$\left[-(2\mathrm{A_{AL}} + \mathrm{A_f})\left(\frac{\mathrm{m}\pi}{\mathrm{a}}\right)^4 - (2\mathrm{A_{AL}}\mathrm{v_{AL}} + \mathrm{A_f}\mathrm{v_f})\left(\frac{\mathrm{m}\pi}{\mathrm{a}}\right)^2\left(\frac{\mathrm{n}\pi}{\mathrm{b}}\right)^2 - 2\big(2\mathrm{A_{AL}}(1-\mathrm{v_{AL}}) + \mathrm{A_f}(1-\mathrm{v_f})\big)\left(\frac{\mathrm{m}\pi}{\mathrm{a}}\right)^2\left(\frac{\mathrm{n}\pi}{\mathrm{b}}\right)^2 - (2\mathrm{A_{AL}}\mathrm{v_{AL}} + \mathrm{A_f}\mathrm{v_f})\left(\frac{\mathrm{m}\pi}{\mathrm{a}}\right)^2\left(\frac{\mathrm{n}\pi}{\mathrm{b}}\right)^2 - (2\mathrm{A_{AL}} + \mathrm{A_f})\left(\frac{\mathrm{n}\pi}{\mathrm{b}}\right)^4\right] \mathrm{w(t)} - (2\rho_{\mathrm{AL}}\mathrm{h_{AL}} + \rho\mathrm{h_f})\frac{\mathrm{d^2w(t)}}{\mathrm{dt^2}} = 0 \tag{33}$$

By comparison, the Equation 33 with Equation 34 can be easily identified as having a simple second-order form, yielding the result ω_n^2 :

$$\frac{d^2w(t)}{dt^2} + \omega_n^2 w(t) = 0 \tag{34}$$

$$\omega_{\mathrm{n}}^2 = \left[-(2\mathrm{A_{AL}} + \mathrm{A_f})\left(\frac{\mathrm{m}\pi}{\mathrm{a}}\right)^4 - (2\mathrm{A_{AL}}\mathrm{v_{AL}} + \mathrm{A_f}\mathrm{v_f})\left(\frac{\mathrm{m}\pi}{\mathrm{a}}\right)^2\left(\frac{\mathrm{n}\pi}{\mathrm{b}}\right)^2 - 2\big(2\mathrm{A_{AL}}(1-\mathrm{v_{AL}}) + \mathrm{A_f}(1-\mathrm{v_f})\big)\left(\frac{\mathrm{m}\pi}{\mathrm{a}}\right)^2\left(\frac{\mathrm{n}\pi}{\mathrm{b}}\right)^2 - (2\mathrm{A_{AL}}\mathrm{v_{AL}} + \mathrm{A_f}\mathrm{v_f})\left(\frac{\mathrm{m}\pi}{\mathrm{a}}\right)^2\left(\frac{\mathrm{n}\pi}{\mathrm{b}}\right)^2 - (2\mathrm{A_{AL}} + \mathrm{A_f})\left(\frac{\mathrm{n}\pi}{\mathrm{b}}\right)^4\right] / -(2\rho_{\mathrm{AL}}\mathrm{h_{AL}} + \rho\mathrm{h_f}) \tag{35}$$

The sandwich used in the research is square such that a=b.

$$\boldsymbol{\omega_n} = \left[\left[-\left(2A_{AL} + A_f\right)\left(\frac{m\pi}{a}\right)^4 - \left(2A_{AL}v_{AL} + A_f v_f\right)\left(\frac{m\pi}{a}\right)^2\left(\frac{n\pi}{a}\right)^2 - 2\left(2A_{AL}(1-v_{AL}) + A_f(1-v_f)\right)\left(\frac{m\pi}{a}\right)^2\left(\frac{n\pi}{a}\right)^2 - \left(2A_{AL}v_{AL} + A_f v_f\right)\left(\frac{m\pi}{a}\right)^2\left(\frac{n\pi}{a}\right)^2 - \left(2A_{AL} + A_f\right)\left(\frac{n\pi}{a}\right)^4\right] / -(2\rho_{AL}h_{AL} + \rho h_f)\right]^{\frac{1}{2}} \tag{36}$$

In the theoretical section, Python was used to calculate the frequencies for each value of n,m=1,3 for the sandwich structure and the vibration modes were plotted as shown in the Figure 5.

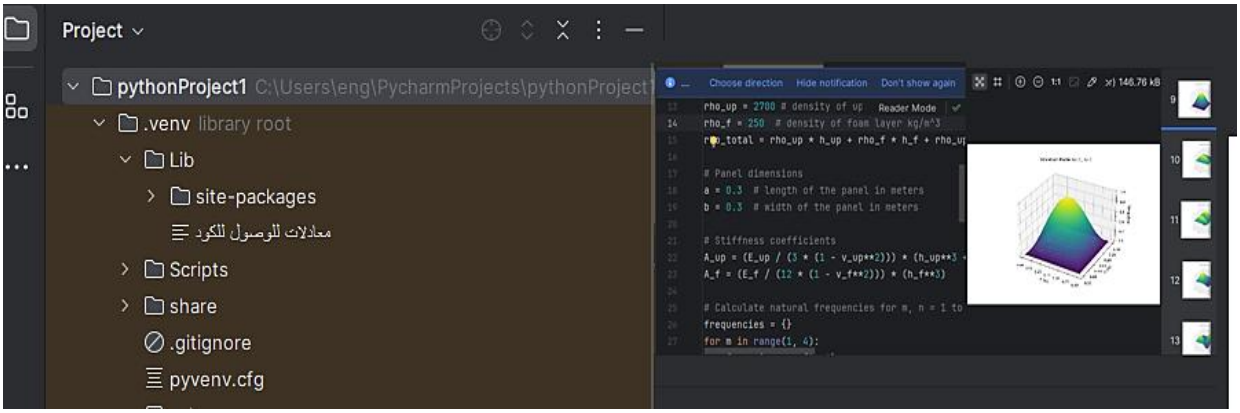

Figure 5: Computational analysis for natural frequencies of a sandwich structure using

4. The numerical investigation of sandwich panel with metal foam core

The accuracy of the proposed analytical solution can be validated using numerical methods. Various numerical techniques are frequently employed for this purpose [32]. ANSYS Design Modeler provides a wide array of advanced modeling capabilities for simulation, including parametric geometry creation, conceptual modeling, automated cleanup and repair, and specialized tools for fluid flow and structural analyses. In this study, the finite element method (FEM), implemented in ANSYS software (version 2021 R1), was used to model the system. A three-dimensional model of a sandwich structure with a metal foam core was developed, applying appropriate boundary conditions to the plate edges for free vibration analysis, as shown in Figure 6. The model was discretized using an 8-node SOLID186 element type with a carefully chosen mesh size, resulting in a total of 36356 elements, as depicted in Figure 7 and Figure 8. The mechanical properties of the metal foam core and the outer layers were assumed to be isotropic and were incorporated into the model under examination. Adhesive constraints were enforced at the interfaces between layers and between the layers and the outer skin of the sandwich panel to prevent [33]. Modal analysis was then performed on the models to identify the free vibration characteristics, such as natural frequencies and mode shapes, based on various parameters, as illustrated in Figure 9.

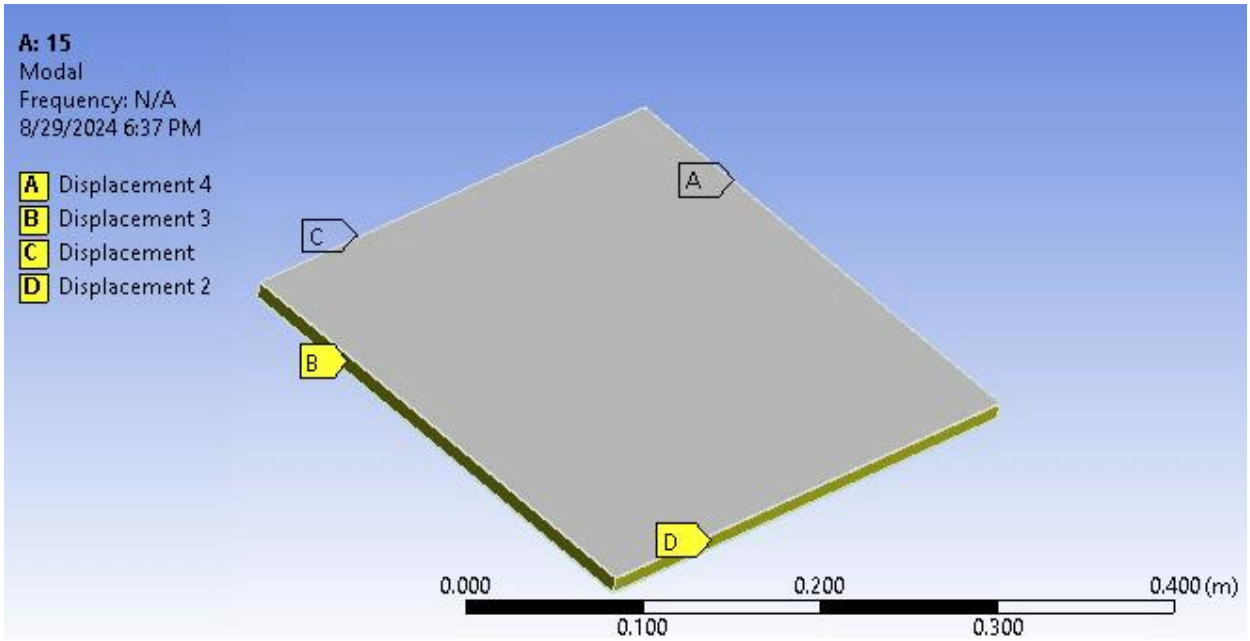

Figure 6: Modal analysis of a simply supported sandwich panel

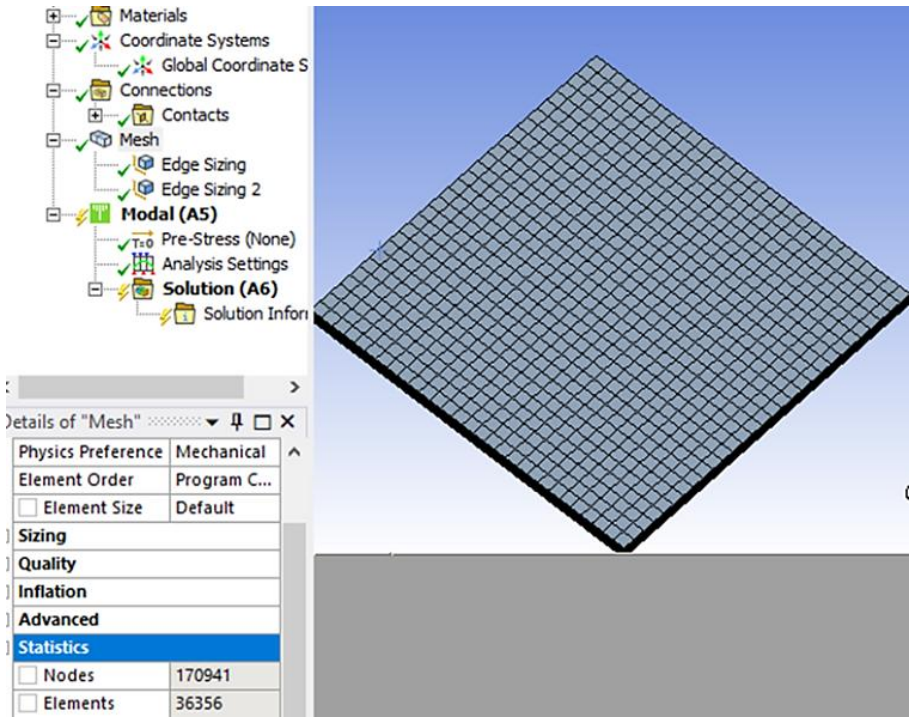

Figure 7: Meshed model for finite element analysis

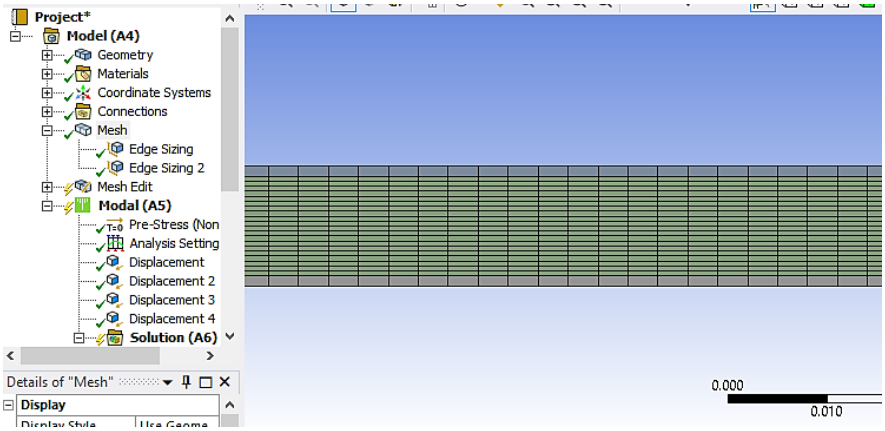

Figure 8: Meshed model for finite element analysis

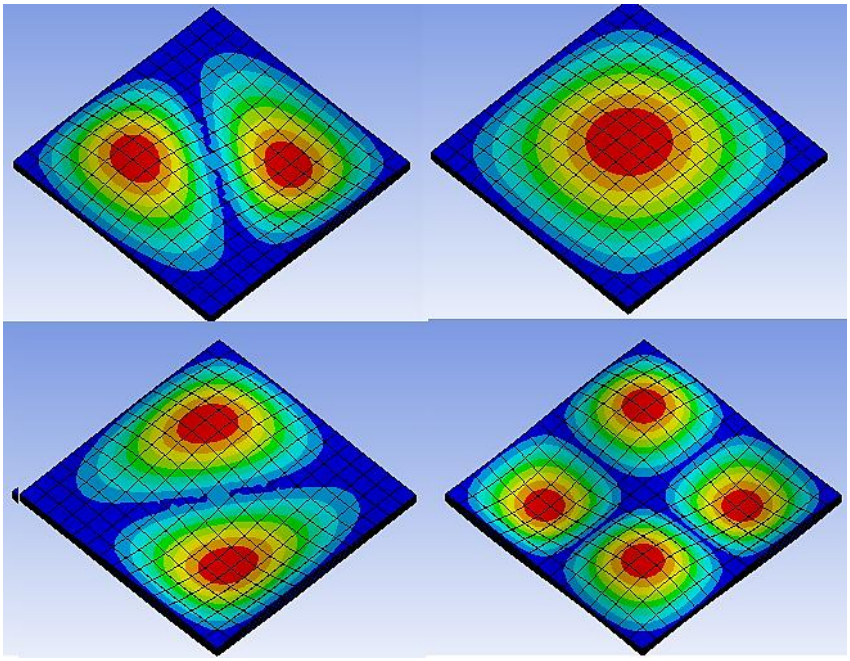

Figure 9: View of modal analysis of metal foam sandwich panel

5. Results and discussion

In this study, a new mathematical model was developed to evaluate the free vibration characteristics of sandwich panels with a metallic foam core, as explained in Equation 36. The effects of various foam core properties, which were theoretically calculated using the Gibson-Ashby model, as explained in Equation 1, were investigated. The natural frequencies of different metallic foam cores were provided based on varying foam densities. Additionally, the available software ANSYS 2021 R1 was used to validate the analytical solution. The obtained results were tabulated and plotted using multiple curves generated through Python programming.

The material properties of the metallic foam core and the corresponding natural frequencies are presented in Table 1. The top and bottom faces of the sandwich panels were made of aluminum, with a mass density of 2700 kg/m³ and Young's modulus of 70 GPa. The panel dimensions of the sandwich are a=300 mm, b=300 mm, thickness of the metal foam =10 mm, and thickness of the aluminum skin =1 mm.

Table 1 shows the natural frequencies calculated both numerically and analytically. The analytical natural frequencies were derived using Equation (36). It was observed that there is a good agreement between the theoretical and numerical results for all values. There was great agreement of the fundamental natural frequency with discrepancies of less than 8.52% as shown Table 1 for the foam density of 350 kg/m³ when n,m=1n, m=1n, m=1. This indicates the accuracy and reliability of both methods in predicting the natural frequencies of the system under investigation. The close match between these approaches validates the model and assumptions used in the theoretical analysis.

The numerical natural frequencies are generally observed to be lower than the theoretical values, which can be attributed to the fact that numerical models account for more realistic deformations and complex stress distributions, aspects that may be overlooked in theoretical models [34]. This is evident in Table 1 and Figure 10. Figure 10 shows that the numerical fundamental natural frequencies follow a similar pattern to the theoretical ones, but with a variation that ranging from 1.14% to 8.52% depending on the case. This suggests that numerical models provide results that are closer to reality compared to theoretical

models, especially when dealing with materials with complex properties, such as metallic foams. The discrepancy between numerical and theoretical results arises because analytical models often simplify assumptions, such as neglecting certain effects (e.g., nonlinear deformations, structural imperfections, and complex dynamic effects). These assumptions can lead to less accurate theoretical results compared to numerical simulations. On the other hand, numerical models (such as those using Finite Element Analysis, or FEA) take into account more material and structural effects, including stress and deformation distribution across the structure, and nonlinear effects [35].

The accuracy of numerical simulations is highly dependent on mesh refinement. In FEA, the structure is divided into small elements (the mesh), as seen in Figure 7 and Figure 8 and the finer the mesh, the more detailed and realistic the results. However, finer meshes also require more computational resources, which increases the time needed for simulations.

Table 1: Numerical and analytical natural frequencies of the metal foam core

Density of aluminum foam Kg/m^3	Elastic modules E_f(Gpa) by Gibson-Ashby	n,m	Numerical Natural frequency (Hz)	Analytical Natural Frequencyn(Hz)	Discrepancies percent %
350	1.18	n=1,m=1	739.66	808.51	8.52
		n=1,m=2	1658.7	2021.28	17.92
		n=2,m=1	1658.7	2021.28	17.94
		n=2,m=2	2428.7	3234.05	24.90
		n=1,m=3	2884.1	4042.56	28.66
		n=3,m=1	2884.1	4042.56	28.66
450	1.94	n=1,m=1	728.97	772.23	5.60
		n=1,m=2	1690.8	1930.58	12.42
		n=2,m=1	1690.8	1930.58	12.42
		n=2,m=2	2535.7	3088.92	17.91
		n=1,m=3	3048.8	3860.79	21.03
		n=3,m=1	3048.8	3860.79	21.03
550	2.9	n=1,m=1	715	742.53	3.71
		n=1,m=2	1695.7	1856.33	8.65
		n=2,m=1	1695.7	1856.33	8.65
		n=2,m=2	2587	2970.13	12.90
		n=1,m=3	3118.5	3712.67	16.00
		n=3,m=1	3118.5	3712.67	16.00
650	4.06	n=1,m=1	700	722.10	3.06
		n=1,m=2	1682	1805.26	6.83
		n=2,m=1	1682	1805.26	6.83
		n=2,m=2	2595	2888.41	10.16
		n=1,m=3	3151	3591.31	12.26
		n=3,m=1	3151	3591.31	12.26
750	5.4	n=1,m=1	687	698.21	1.61
		n=1,m=2	1667	1745.53	4.50
		n=2,m=1	166	1745.53	4.50
		n=2,m=2	2586	2792.84	7.41
		n=1,m=3	3101.8	3491.05	11.15
		n=3,m=1	3101.8	3491.05	11.15
850	6.94	n=1,m=1	674	681.75	1.14
		n=1,m=2	1645	1704.39	3.48
		n=2,m=1	1645	1704.39	3.48
		n=2,m=2	2569	2727.02	5.79
		n=1,m=3	3094.8	3408.77	9.21
		n=3,m=1	3094.8	3408.77	9.21
1000	9.6	n=1,m=1	652.26	662.41	1.53
		n=1,m=2	1595.	1656.03	3.69
		n=2,m=1	1595.	1656.03	3.69
		n=2,m=2	2499.	2649.65	5.69
		n=1,m=3	3081.9	3312.06	6.95
		n=3,m=1	3081.9	3312.06	6.95

Influence of Density on Natural Frequencies is shown in Table 1 and Figure 10 and Figure 11. The effect of density on natural frequency is clearly noticeable. As the material density increases, the natural frequency decreases. For instance, at a density of 350 kg/m³, the theoretical natural frequency for the mode (n=1, m=1) is 808.51 Hz, while at 1000 kg/m³, the theoretical frequency drops to 662.41 Hz. The relationship between stiffness and mass can explain this decrease in frequency with increasing density [36]. Gibson and Ashby [26], explained the relationship between density and stiffness in cellular materials like metallic foam, where mass increases with density, leading to a decrease in the natural frequencies of structures. This aligns with the findings of the current study, where increasing density results in lower natural frequencies. Similarly, Ashby et al. [37], examined

the effect of density on structural properties and found that higher-density materials reduce natural frequencies due to increased mass, reinforcing the concept of balancing mass and stiffness for optimal performance. Gao et al. [8], confirmed the inverse relationship between density and natural frequencies, supporting the theoretical and numerical results obtained. Finally, Elettore [38] demonstrated that panels with lower densities exhibit higher natural frequencies than those with higher densities. All of these previous studies corroborate the findings of our current study.

However, lower densities (350-450 kg/m³) may be advantageous in scenarios where reducing weight is crucial. Despite a higher discrepancy (8.52% at 350 kg/m³), lower densities are beneficial in lightweight applications, like automotive and aerospace design. Thus, the optimal density selection depends on the specific requirements: higher densities are ideal for precision, while lower densities are suitable when weight reduction is a priority. On the other hand, the increase in Young's modulus, which rises with increasing density, directly affects the natural frequency of structures. The natural frequency of any system depends on both mass and stiffness, and Young's modulus is a measure of material stiffness. As Young's modulus increases, the stiffness of the material also increases, meaning the material becomes more resistant to deformation when subjected to external loads.

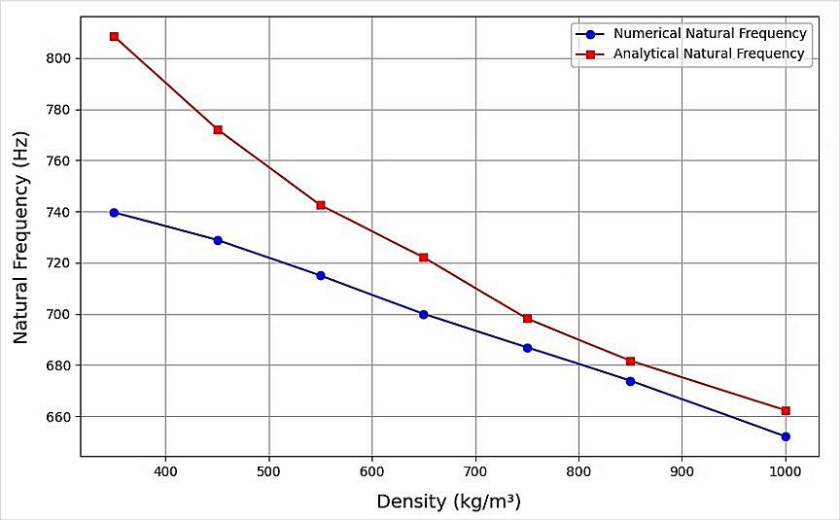

Figure 10: Relationship between density with analytical and numerical natural frequencies

Recent research supports the relationship between Young's modulus and natural frequency, showing that as Young's modulus increases, the material's stiffness also increases, leading to higher natural frequencies, assuming mass remains constant. A study conducted on composite materials reinforced with shape memory alloy confirmed this effect, where increased stiffness resulted in a significant rise in the natural frequency [26]. This reinforces the correlation between stiffness, Young's modulus, and natural frequencies.

The vibration mode analysis of aluminum foam composite panels was conducted using both analytical models and numerical simulations, as shown in Figure 12 (a-f) and Figure 13 (a-f). The graphs derived from numerical analysis (generated using ANSYS software) and theoretical calculations (computed using Python) illustrate the natural vibration behavior of the composite panel. These graphs illustrate the varying vibration patterns of the sandwich as the constants n and m are altered. The primary purpose of these graphs is to simulate the behavior of the composite panel under free vibrations. These visual representations provide insight into the deformation patterns and displacements that occur on the surface of the panel at each natural frequency. The graphs assist engineers in identifying vibration modes (mode shapes) and the corresponding natural frequencies in the system.

The Python-generated graphs aim to compare the natural frequencies calculated analytically (using theoretical equations) with those obtained numerically through ANSYS. This comparison helps ensure the accuracy of the theoretical models and validates their results against numerical data. The Python plots also show the relationship between density and natural frequency, which aids in optimizing the panel design based on material properties such as density and Young's modulus.

The identification of vibration modes is crucial for detecting critical resonances that may lead to mechanical failure or permanent deformation of the panel [32]. By analyzing these modes, engineers can improve the structural design to enhance resistance to detrimental vibrations, thus extending the lifespan of components made from aluminum foam. Comparing the numerical and analytical results vibration modes must be identified to detect critical resonances that could cause panel failure or permanent deformation. Analyzing these modes allows engineers to improve the structural design to reduce vibrations and extend aluminum foam component the lifespan. Free vibration analysis optimizes panel density and stiffness for aerospace and automotive applications. Ensuring the accuracy of the theoretical models and confirms their alignment with real-world behavior, when the results closely match, engineers can rely on the analytical models to perform calculations more efficiently, saving time and effort. This validation process helps ensure that theoretical approaches are reliable for future use in design and analysis. Although the numerical and analytical models yielded promising results, it is important to note that the model is based on Classical Plate Theory, which assumes a specific thickness and material homogeneity. This approach is commonly accepted in studies involving metallic foams for simplification purposes. However, these assumptions may not accurately capture the

behavior in more complex applications, as the model employs simply supported boundary conditions. Consequently, the generalizability of the findings to other structures is limited, particularly as the study focused only on different densities of homogeneous metallic foam.

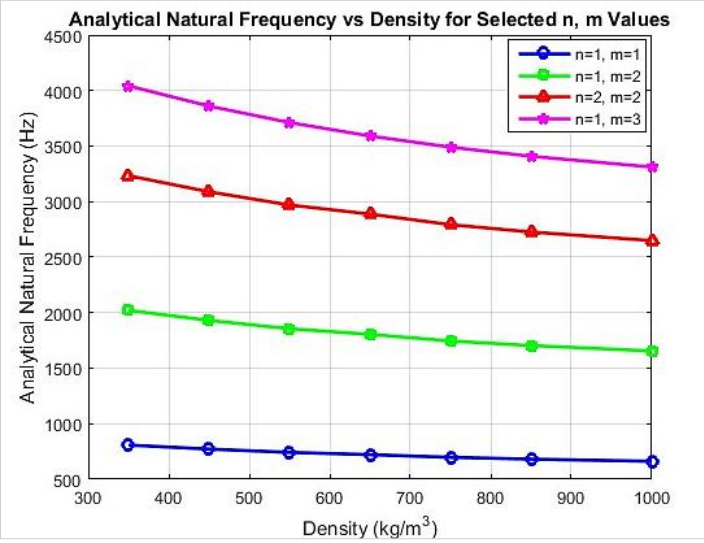

Figure 11: Analytical natural frequency at diffrent n,m

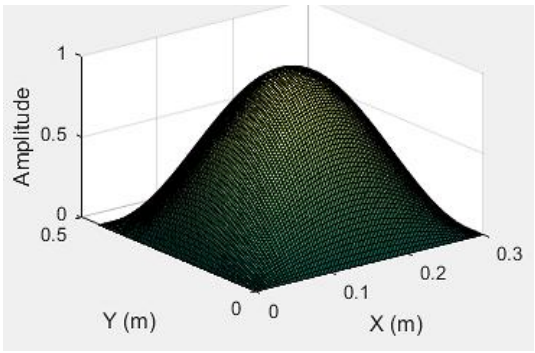

(a) mode shape at n=1, m=1

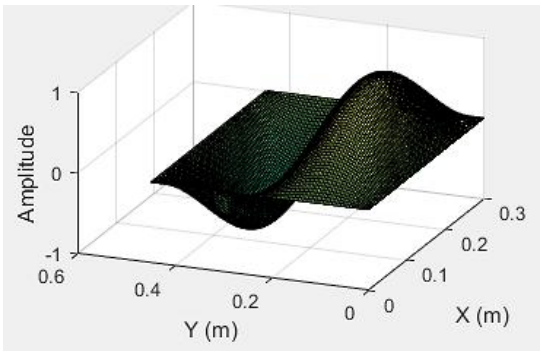

(b) mode shape at n=1, m=2

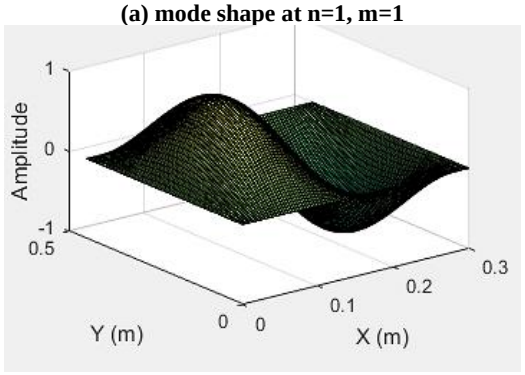

(c) mode shape at n=2, m=1

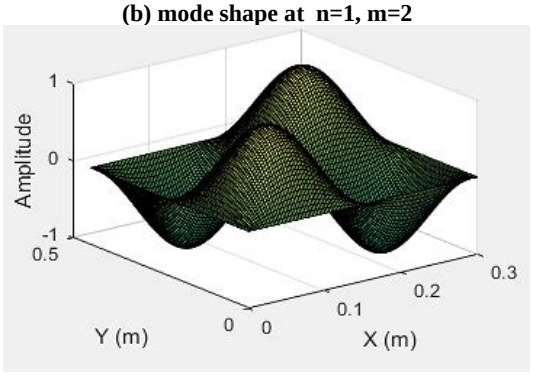

(d) mode shape at n=2, m=2

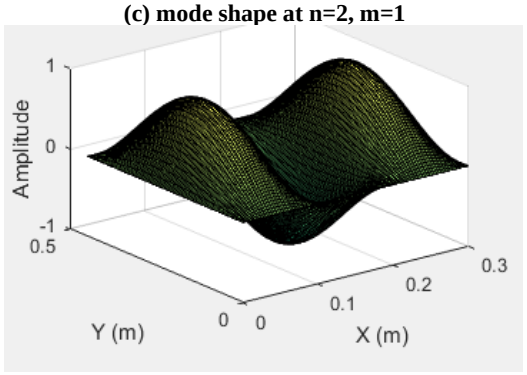

(e) mode shape at n=1, m=3

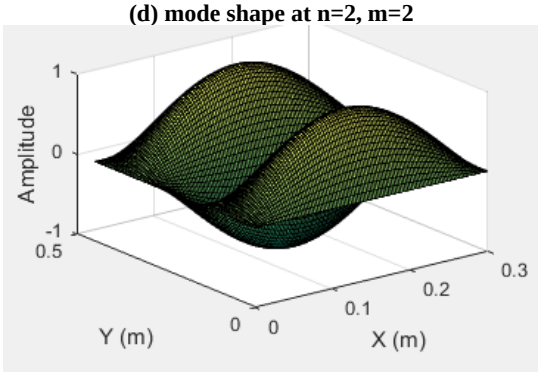

(f) mode shape at n=3, m=1

Figure 12: Effect of varying mode numbers (n, m) on analytical natural frequencies of aluminum foam sandwich panel

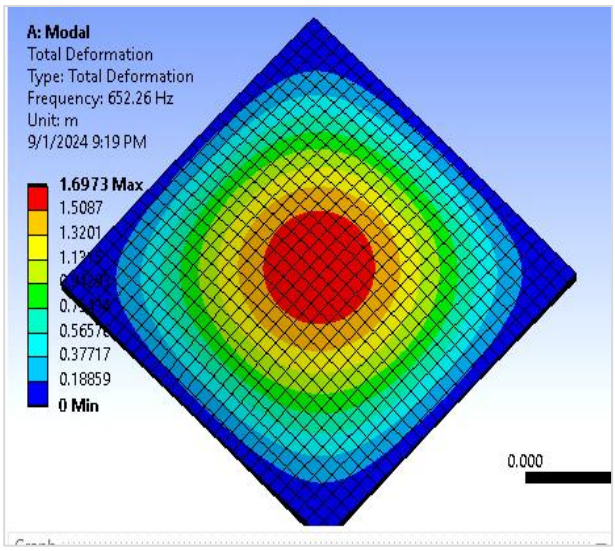

(a) mode shape at n=1, m=1

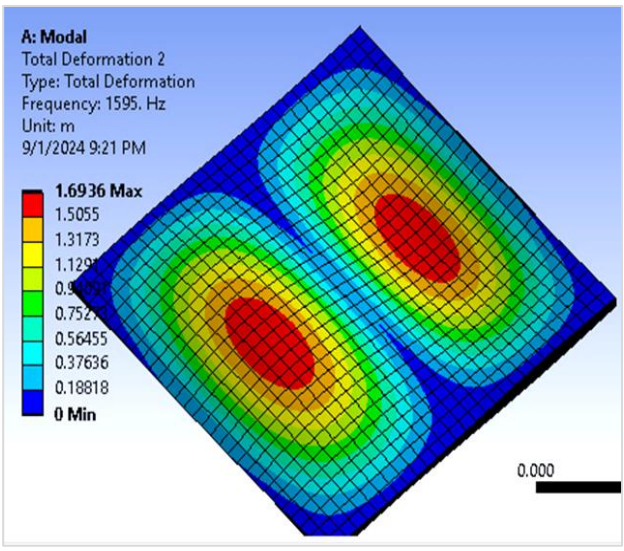

(b) mode shape at n=1, m=2

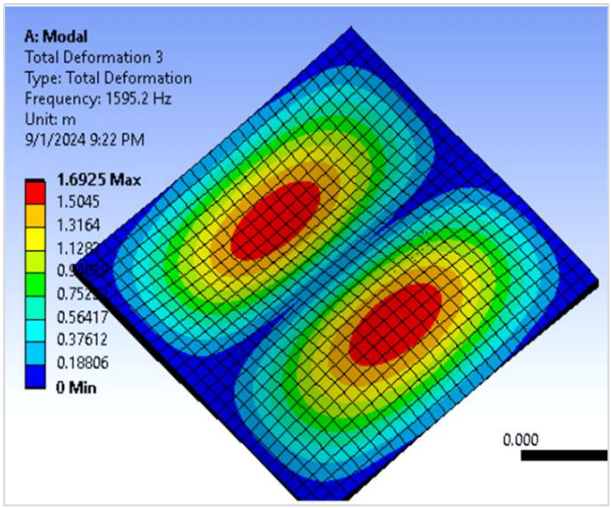

(c) mode shape at n=2, m=1

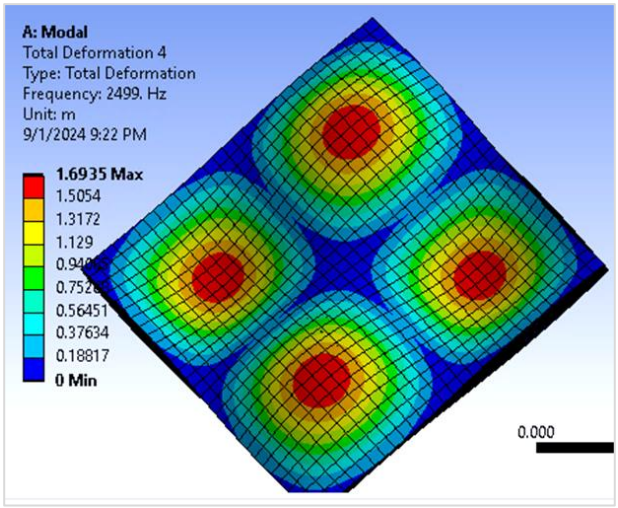

(d) mode shape at n=2, m=2

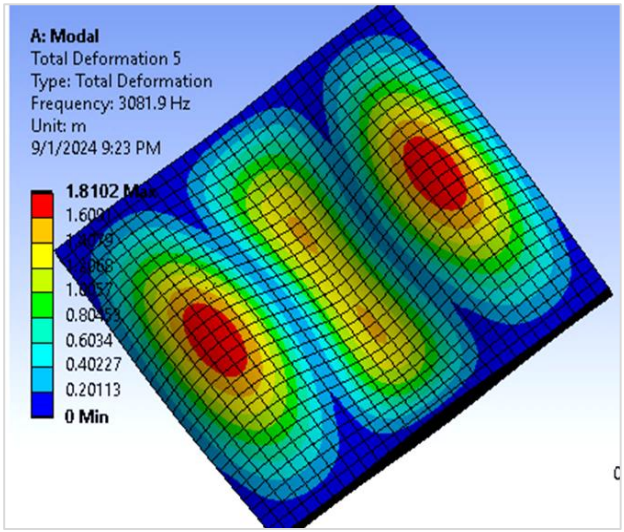

(e) mode shape at n=1, m=3

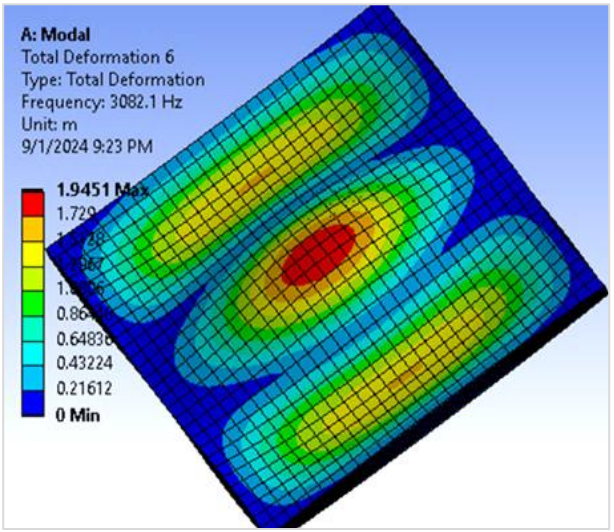

(f) mode shape at n=3, m=1

Figure 13: Mode shape of aluminum foam sandwich panel with density foam 1000 kg/m^3 using ANSYS

6. Conclusion

This study demonstrated that aluminum foam sandwich panels exhibit excellent vibrational properties, making them highly suitable for lightweight structural applications. The comparison between numerical and analytical models showed a strong correlation, validating the analytical approach.

Key findings include:

1) The study developed a mathematical model using Classical Plate Theory (CPT) to predict the natural frequencies of sandwich panels with an aluminum foam core. The model was validated using Finite Element Analysis (FEA) in ANSYS, demonstrating strong agreement between analytical and numerical results.
2) Increasing the foam density decreases natural frequencies due to the added mass, while a higher Young's modulus increases stiffness, resulting in higher frequencies.
3) The optimal density range of 750-1000 kg/m³ provided the smallest discrepancies (1.14%) between numerical and analytical models, indicating its suitability for applications requiring vibrational stability and precision.
4) Although higher densities offer precision in vibrational stability, lower densities (350-450 kg/m³) are advantageous for applications prioritizing weight reduction.

Author contributions

Conceptualization, **Z. Hamdan, M. Jweeg** and **S. Bakhy**; data curation, **Z. Hamdan**; formal analysis, **Z. Hamdan**; investigation, **Z. Hamdan**; methodology, **S. Bakhy**; project administration, **M. Jweeg**; resources, **M. Jweeg**; software, **Z. Hamdan**; supervision, **M. Jweeg**; validation, **Z. Hamdan**, **S. Bakhy**, and **M. Jweeg**; visualization, **Z. Hamdan**; writing—original draft preparation, **Z. Hamdan**; writing—review and editing, **S. Bakhy** and **M. Jweeg**. All authors have read and agreed to the published version of the manuscript.

Funding

This research received no specific grant from any funding agency in the public, commercial, or not-for-profit sectors.

Data availability statement

The data that support the findings of this study are available on request from the corresponding author.

Conflicts of interest

The authors declare that there is no conflict of interest.

References

[1] A. E. Simone, L. J. Gibson, Aluminium foams produced by liquid state processes, Acta Mater., 46 (1998) 3109-3123. https://doi.org/10.1016/S1359-6454(98)00017-2

[2] B. Parveez, N. A. Jamal, H. Anuar, Y. Ahmad, A. Aabid, M. Baig, Microstructure and mechanical properties of metal foams fabricated via melt foaming and powder metallurgy technique: A Review, Materials, 15 (2022) 5302. https://doi.org/10.3390/ma15155302

[3] S. Sahu, D. P. Mondal, J. U. Cho, M. D. Goel, M. Z. Ansari, Low-velocity impact characteristics of closed cell AA2014-SiCp composite foam, Compos. B Eng., 160 (2019) 394- 401. https://doi.org/10.1016/j.compositesb.2018.12.054

[4] A. K. Shukla, J. D. Majumdar, Studies on microstructure and mechanical properties of aluminium foam prepared by spray forming route, Procedia Manuf., 35 (2019) 861-865. http://dx.doi.org/10.1016/j.promfg.2019.06.032

[5] D. Rui, M. Wang, D. Wang, H. Zengrong, M. D. Green, Q. Nian, Understanding mechanical behaviour of metallic foam with hollow struts using the hollow pentagonal dodecahedron model, Scr. Mater., 182 (2020) 114-119. https://doi.org/10.1016/j.scriptamat.2020.03.001

[6] D. K. Rajak, L. A. Kumaraswamidhas, S. Das, An energy absorption behaviour of foam filled structures, Procedia Mater. Sci., 5 (2014) 164-172. http://dx.doi.org/10.1016/j.mspro.2014.07.254

[7] R. Karuppasamy, D. Barik, Production methods of aluminium foam: A brief review, Mater. Today, Proc., 37 (2021)1584-1587. https://doi.org/10.1016/j.matpr.2020.07.161

[8] Q. Gao, X. Su, Z. Feng, P. Huang, Z. Wei, X. Sun, G. Zu, Preparation, bubbles evolution, and compressive mechanical properties of copper-coated carbon fibers/aluminum foam sandwich panels, J. Mater. Res. Technol., 30 (2024) 375- 384. http://dx.doi.org/10.1016/j.jmrt.2024.03.048

[9] E. Elettore, M. Latour, M. D'Aniello, R. Landolfo, G. Rizzano, Prototype Tests on Screwed Steel–Aluminium Foam–Steel Sandwich Panels, Buildings, 13 (2023) 2836. https://doi.org/10.3390/buildings13112836

[10] P. Huang, Q. Gao, X. Su, Z. Feng, X. Sun, G. Zu, Effect of Core Density on the Three-Point Bending Performance of Aluminum Foam Sandwich Panels, Materials, 16 (2023) 7091. https://doi.org/10.3390/ma16227091

[11] A. Sato, M. Latour, M. D'Aniello, G. Rizzano, R. Landolfo, Experimental response of full-scale steel-aluminium foam-steel sandwich panels in bending, ce/papers, 6 (2023) 452- 457. https://doi.org/10.1002/cepa.2710

[12] A. Vidwans, P. Trovalusci, N. Fantuzzi, J. A. Correia, Application of column buckling theory to steel aluminium foam sandwich panels, Structures, 54 (2023) 607- 617. https://doi.org/10.1016/j.istruc.2023.04.112

[13] R. Selvaraj, A. Maneengam, M. Sathiyamoorthy, Characterization of mechanical and dynamic properties of natural fiber reinforced laminated composite multiple-core sandwich plates, Compos. Struct., 284 (2022) 115141. https://doi.org/10.1016/j.compstruct.2021.115141

[14] P. Mohammadkhani, S. S. Jalali, M. Safarabadi, Experimental and numerical investigation of Low-Velocity impact on steel wire reinforced foam Core/Composite skin sandwich panels, Compos. Struct., 256 (2021) 112992. https://doi.org/10.1016/j.compstruct.2020.112992

[15] M. Al-Waily, M. A. Al-Shammari, M. Jweeg, An Analytical Investigation of Thermal Buckling Behavior of Composite Plates Reinforced by Carbon Nano Particles, Eng. J., 24 (2020) 11-21. http://dx.doi.org/10.4186/ej.2020.24.3.11

[16] P. Huang, Q. Gao, X. Su, Z. Feng, X. Sun, G. Zu, Effect of Core Density on the Three-Point Bending Performance of Aluminum Foam Sandwich Panels, Materials, 16 (2023) 7091. https://doi.org/10.3390/ma16227091

[17] V. O. Babarinde, I. Telichev, Augmenting foam-core sandwich panel with toughened blanket for enhanced orbital debris protection, Int. J. Impact Eng., 182 (2023)104772. https://doi.org/10.1016/j.ijimpeng.2023.104772

[18] A. Mouthanna, S. H. Bakhy, M. Al-Waily, A Computer Presentation of the Analytical and Numerical Study of Nonlinear Vibration Response for Porous Functionally Graded Cylindrical Panel, Adv. Eng. Technol. Appl., 1983 (2023) 57-72. https://doi.org/10.1007/978-3-031-50920-9_5

[19] M. Amir, K. Sang-Woo, L. Soo-Yong, Free vibration analysis of the geometrically nonlinear functionally graded porous curved panels in deterministic and stochastic domains considering various boundary conditions, Waves Random Complex Medium, (2024) 1- 26. https://doi.org/10.1080/17455030.2024.2343100

[20] E. K. Njim, S. H. Bakhy, M. Al-Waily, Analytical and Numerical Investigation of Free Vibration Behavior for Sandwich Plate with Functionally Graded Porous Metal Core, Pertani. J. Sci. Technol., 29 (2021) 2475-2021. http://dx.doi.org/10.47836/pjst.29.3.39

[21] D. P. T. Minh, N. N. Khoa, S. Nguyen-Van, N. T. Hoa, N. Nguyen-Dinh, N. Q. Hung, L. V. Dung, A Numerical Model for the Composite Sandwich Panel in Vibration by the Homogenization Method, Adv. Eng. Res., 366 (2022) 79-88. http://dx.doi.org/10.1007/978-3-030-92574-1_8

[22] F. Djamaluddin, Optimization of Free Vibration for Sandwich Foam Core, Int. J. Mech., 17 (2023) 93-98. http://dx.doi.org/10.46300/9104.2023.17.14

[23] Y. Q. Wang, J. W. Zu, Vibration behaviors of functionally graded rectangular plates with porosities and moving in thermal environment, Aerosp. Sci. Technol., 69 (2017) 550-562. https://doi.org/10.1016/j.ast.2017.07.023

[24] B. Badarloo, H. Salehipour, An analytical closed-form solution for free vibration and stability analysis of curved sandwich panels made of porous metal-foam core and nanocomposite reinforced face-sheets, Proc. Inst. Mech. Eng. C, J. Mech. Eng. Sci., 238 (2023) 2969-2987. https://doi.org/10.1177/09544062231195491

[25] O. Rahmani, K. Malekzadeh, S. Mohammad, S. M. R. Khalili, Analytical Solution for Free Vibration of Sandwich Structures with a Functionally Graded Syntactic Foam Core, Mater. Sci. Forum., 636-637 (2010) 1143-1149. https://doi.org/10.4028/www.scientific.net/MSF.636-637.1143

[26] Michael F. A. and Cellular, M. F., Solids: Structure and Properties (2nd ed.), Cambridge University Press, 1997.

[27] D. Duryodhana, S. Waddar, D. Bonthu, J. Pitchaimani, S. Powar, M. Doddamani, Buckling and free vibrations behaviour through differential quadrature method for foamed composites, Results in Engineering, 17 (2023) 100894. https://doi.org/10.1016/j.rineng.2023.100894

[28] M. F. Ashby, A. Evans, N. A. Fleck, L. J. Gibson, J. W. Hutchinson, H. N. G. Wadley, Metal foams: a design guide: Butterworth-Heinemann, Oxford, UK, ISBN 0-7506-7219-6, Published 2000, Hardback, 251 pp., $75.00, Mater. Des., 23 (2002) 119. http://dx.doi.org/10.1016/S0261-3069(01)00049-8

[29] Ventsel, E. and Krauthammer, T., Thin Plates and Shells, CRC Press, Boca Raton, 1st edition, 2001.

[30] M. Al-Waily, M. A. Al-Shammari, M. J. Jweeg, An analytical investigation of thermal buckling behavior of composite plates reinforced by carbon nano-part icles, Eng. J., 24 (2020) 11-21. http://dx.doi.org/10.4186/ej.2020.24.3.11

[31] A. W. Leissa, Vibration of plates Scientific and Technical Information Division, National Aeronautics and Space Administration. 160 (1969).

[32] S. E. Sadiq, M. J. Jweeg, and S. H. Bakhy, The effects of honeycomb parameters on transient response of an aircraft sandwich panel structure. In IOP Conference Series, Mater. Sci. Eng., 928 (2020) 022126. https://doi.org/10.1088/1757-899X/928/2/022126

[33] V. N. Burlayenko, V. N., and T. Sadowski, Free vibrations and static analysis of functionally graded sandwich plates with three-dimensional finite elements. Meccanica, 55 (2020) 815-832. https://doi.org/10.1007/s11012-019-01001-7

[34] J. Urruzola, I. Garmendia, Improved FEM Natural Frequency Calculation for Structural Frames by Local Correction Procedure, Buildings 14 (2024) 1195. https://doi.org/10.3390/buildings14051195

[35] Pandimani, Ponnada, M. R., and Y. Geddada, Numerical nonlinear modeling and simulations of high strength reinforced concrete beams using ANSYS, J. Build. Pathol. Rehabil., 7 (2022) 22. https://doi.org/10.1007/s41024-021-00155-w

[36] F. Boutaghane, H. Aouici, and A. M. Bouchelaghem, Classification of the vibration conditions on the natural frequency and the maximal displacement using response surface methodology (RSM). Int. J. Adv. Manuf. Technol., 103 (2019) 4495-4505. https://doi.org/10.1007/s00170-019-03867-z

[37] Ashby, M. F., Evans, A. G., Fleck, N. A., Gibson, L. J., Hutchinson, J. W., & Wadley, H. N. G. Metal Foams: A Design Guide. Butterworth-Heinemann, 2000.

[38] E. Elettore, M. Latour, M. Aniello, R. Landolfo, & G. Rizzano, Prototype Tests on Screwed Steel–Aluminium Foam–Steel Sandwich Panels, Buildings, 13 (2023) 2836. https://doi.org/10.3390/buildings13112836